INTERNATIONAL JOURNAL OF CLIMATOLOGY
RMetS Royal Meteorological Society

Cold-air pool evolution in a wide Pyrenean valley

Journal:	*International Journal of Climatology*
Manuscript ID	JOC-17-0159.R2
Wiley - Manuscript type:	Research Article
Date Submitted by the Author:	18-Jan-2018
Complete List of Authors:	Conangla, Laura; Universitat Politècnica de Catalunya, Department of Mining, Industrial and ICT Engineering Cuxart, Joan; University of the Balearic Islands, Physics Jiménez, Maria Antonia; University of the Balearic Islands, Physics Martínez-Villagrasa, Daniel ; University of the Balearic Islands, Physics Miró, Josep Ramon; Meteorological Service of Catalonia, Applied Research and Modelling Tabarelli, Davide; University of Trento, Department of Civil, Environmental and Mechanical Engineering Zardi, Dino; University of Trento, Department of Civil, Environmental and Mechanical Engineering
Keywords:	Cold-air pool, Drainage flow, Mesoscale simulation, Pyrenean wide plain, Stable boundary layer, Turbulence
Country Keywords:	Spain, France

SCHOLARONE™
Manuscripts

Cold-air pool evolution in a wide Pyrenean valley

Laura Conangla[1](*), Joan Cuxart[2], Maria Antonia Jiménez[2], Daniel Martínez-Villagrasa[2], Josep Ramon Miró[3], Davide Tabarelli[4], Dino Zardi[4]

[1] Department of Mining, Industrial and ICT Engineering. Polytechnic University of Catalonia. Manresa, Spain.

[2] Department of Physics. University of the Balearic Islands. Palma de Mallorca, Spain.

[3] Servei Meteorològic de Catalunya. Barcelona, Spain.

[4] Atmospheric Physics Group, Department of Civil, Environmental and Mechanical Engineering, University of Trento, Trento, Italy.

(*) Avinguda de Les Bases de Manresa 61-73, 08242 Manresa, Spain, laura.conangla@upc.edu, +34 93 877 72 76

Peer Review Only

Abstract

This study on cold-air pool formation in the wide Cerdanya Valley in the Pyrenees mountain range was conducted using available observational information from September 2010 to August 2014. Cold-air pools occur during almost 60% of the nights, mainly during winter. Cold pools develop even under significant synoptic pressure gradients. Additionally, drainage currents transporting air down-valley occur most of the nights. In particular one representative cold-air pool event has been analyzed in detail by a high-resolution mesoscale simulation, combined with an analysis of data from both ground-based stations and satellites. Radiative processes dominate the

http://mc.manuscriptcentral.com/joc

evolution of cold-air pools, together with turbulence in the lowest layers, while drainage flows down from the high mountains mainly through the tributary valleys and from the valley sidewall slopes play a key role in bringing air to the pool. Cold pool formation begins approximately one hour after sunset, and it extends across most of the valley bottom, with a very strong thermal inversion close to the surface that has a depth of up to one hundred meters in the lowest parts of the valley. Wind veers down-valley along the main axis two to three hours after sunset and the wind direction is approximately maintained until after sunrise.

Key words: Cold-air pool · Drainage flow · Mesoscale simulation · Pyrenean wide valley · Stable boundary layer · Turbulence

Peer Review Only

1. INTRODUCTION

A cold-air pool (CAP) may be defined as a topographically confined stagnant layer of air that is colder than the air above it. This definition does not specify the air temperature difference between the stagnant layer and the air above or the height of these reference layers. Iijima and Shinoda (2000), considering a CAP formation in an elevated hollow, concluded that it occurred when a maximum temperature inversion between the bottom of the hollow (2230 m above sea level (asl)) and the summit of the hollow (2380 m asl) of more than 2 °C exists (namely, a vertical gradient of 1.33 °C/100 m), for at least 2 h.

Peer Review Only

CAPs can be characterized as diurnal, forming during the evening or night and decaying after sunrise the next day, or as persistent, when they last for several days (Zardi and Whiteman, 2013). CAPs in sinkholes and valleys have been extensively examined over the past few decades, but the mechanisms of their formation and evolution are not fully understood and still poorly modeled. The difference between the temperature at the valley bottom and outside the valley can be several degrees (Jiménez *et al.*, 2015; Martínez *et al.*, 2010; Smith *et al.*, 2010), reaching up to 20 degrees difference in closed sinkholes (Clements *et al.*, 2003; Iijima and Shinoda, 2000).

Furthermore, CAPs can be found at other scales or topographical forms. For instance, there is some literature addressing very large persistent CAPs forming in North America west of the Rocky Mountains (Yu *et al.*, 2017; Zhong *et al.*, 2001). To exist and be persistent, these basin-wide CAPs require a temperature inversion with its top near the mountain-range summit levels, presenting a double-inversion structure, with one near the ground and another above it. These CAPs could be disturbed by a passing shortwave trough and removed by turbulent mixing and a strong wind shear (Lareau and Horel, 2015).

Studies in the Duero basin NW of the Iberian Peninsula (Martínez *et al.*, 2010) show that wide-basin CAP-like structures can form at the basin-scale for a diurnal cycle, allowing the development of mesoscale structures above them (Cuxart, 2008). Moreover, smaller CAPs over shallow terrain depressions can also be formed inside the main CAP, leading to significant variation of the air temperature near the surface within one single CAP.

A CAP usually consists of a strongly stratified layer that is in contact with the surface, with a thickness of tens to a few hundred meters; in valleys, groups of trees or terrain undulations create sheltered areas that favor CAP formation. This effect reduces the turbulent mixing above the air adjacent to the ground, leading to a rapid cooling of the air close to the radiatively cooling surface (Gustavsson *et al.*, 1998; Vosper and Brown, 2008). Pollutants released within a CAP may stay trapped within them, causing potential health hazards in areas with heavy traffic or industries (Young and Whiteman, 2015). CAPs are often the coldest spots of a region, and this implies enhanced heating needs for households in these areas.

Stagnant stable boundary layers are a challenge for numerical weather prediction and for climate studies, because extremely weak wind and turbulence are very difficult to address with the current physical parameterizations. Sometimes parameterization schemes generate too low air temperatures because the surface radiative cooling is not properly transported upward due to insufficient turbulent mixing which can lead to unrealistic too low values of temperature near the ground ("run-away cooling", Viterbo

Peer Review Only

et al. (1999)). In some configurations, to avoid excessive cooling near the surface, the turbulence scheme is set to mix in excess, resulting in too high a temperature near the ground. Therefore, an adequate forecast of the near surface temperature in models is still a challenge for stable nights (Cuxart *et al.*, 2006; Holtslag *et al.*, 2013).

The Cerdanya Valley in the Pyrenees is a location where the minimum absolute temperature for Catalonia occurs very often, a country that has a very diverse topography, with coastal areas, several mountain ranges and a large continental plain. Forecasts of the minimum temperature are usually overestimated in value for stably stratified conditions by several degrees (Pagès and Miró, 2010). The valley has a number of weather stations, and it is visible from satellites (section 2). Therefore, this area was selected for this study on the characteristics of CAPs that form there. First the available data were statistically analyzed (section 3), and then, the evolution of the CAP was identified, along with its interaction with the flows coming from the surrounding topographical structures, by a high-resolution numerical simulation (section 4).

Peer Review Only

2. MATERIALS AND METHODS

2.1 Study area

The Pyrenees mountain range is in southwestern Europe, forming a natural border between the Iberian Peninsula and the rest of Europe that stretches from the shores of the Mediterranean Sea to the Bay of Biscay on the Atlantic Ocean. Pyrenean valleys are mostly oriented from north to south, perpendicularly to the axis of the mountain range. The Cerdanya Valley, which is the subject of this study, is oriented from ENE to WSW, parallel to the axis of its surrounding mountains, as shown in Figure 1a.

http://mc.manuscriptcentral.com/joc

The Cerdanya Valley is well-defined as the headwaters of the Segre River that circulates from east to west. It has a considerably wide valley floor approximately 35 km long and 9 km wide, at most, with the bottom between 1300 m and 950 m asl, declining in the direction of that the Segre River flows. The valley floor is surrounded by the main axis of the Pyrenees in the north with peaks over 2900 m asl (Carlit and Puigpedrós sub-ranges); by the Cadí and Moixeró sub-ranges in the south, peaking at 2649 m asl; and by the Puigmal sub-range (2910 m asl) in the SE. Long narrow valleys represent the tributaries on the northern side (Angostrina, Querol, Duran and La Llosa), whereas on the southern side, steep slopes dominate, with the La Molina valley as the main tributary. This topographic distribution plays a crucial role in the generation of slope and along-valley winds as will be discussed in section 4.

The microclimate of the Cerdanya Valley is based on its orientation that follows the path of the sun; thus, it is sunnier and drier compared to other Pyrenean valleys. Sunshine hours are among the highest in Europe at approximately 3000 hours per year. According to the data of the Meteorological Service of Catalonia, the annual rainfall varies from 600 to 700 mm at the valley floor and from 1000 to 1200 mm in the upper mountains. This difference is associated with the fact that the highest summits retain the precipitation from Atlantic storms along the north slope of the Pyrenees and the humid air of the Mediterranean Sea on its south slope, raining less on the valley floor. Spring and summer are the rainiest seasons. The main snowfall events, with snow reaching the valley bottom, tend to be in January and February. The snow remains on the ground for many days in the shaded areas and melts quickly in the sunny areas.

Peer Review Only

The temperature range at the bottom of the valley is large, with high daily and annual thermal amplitudes, and a strong thermal inversion in winter. The thermal amplitude is lower in the mountains, depending on the altitude and orientation of each location.

The vegetation can be categorized into three types, according to altitude. The mountain level (below 1600 m asl), enclosing the wide valley floor, is covered by pastures and patches of beech forests on the shaded slopes and oaks and Scots pines on the sun-facing slopes, with box in the undergrowth. At the subalpine level (from 1600 to 2000 m asl), there are fir trees on the shaded slopes and mountain pine on the opposite slopes. The alpine level or the highest areas are covered only by alpine meadows.

2.2 Experimental data and data processing

a. Automatic weather stations

Six automatic weather stations (AWS) are permanently operated over the Cerdanya Valley, in the positions shown in Figure 1b, by the Meteorological Service of Catalonia (SMC), the French National Meteorological Service (Météo-France) and the Spanish Meteorological Agency (AEMET).

Three of the stations are at the bottom of the valley from east to west, one in Santa Llocaia (SL) operated by Météo-France at the foothills of the SE range, one in Das (DA) operated by SMC in a very wide and flat area, and one in Martinet (MR) operated by AEMET, where the valley begins to narrow. Between Das and Martinet, there is an elevated area that separates the valley floor into two subparts, of approximately 200 m above the average altitude of the bottom area, leaving a very narrow step for air

Peer Review Only

circulation at the river pass. On the other hand, the other three stations are in mountain areas: one in Malniu (ML) operated by SMC, at the northeast of Das, surrounded by coniferous vegetation; one in Cadí Nord (CN) operated by SMC near the ridge at the south slope; and one in La Molina (LM) operated by AEMET, on a poorly vegetated slope in the southern mountains.

A four-year period (01/09/2010 - 31/08/2014), named the "study period", was analyzed, with measurements of temperature and relative humidity at 1.5 m above ground level (agl), wind speed and direction at 10 m agl (except the AWS at Malniu, where the wind is measured at 6 m agl) and global solar radiation at Das. This period included data for all the stations, of which some were new. Even if it is short, it provides some indications on the behavior of the CAP in La Cerdanya Valley that are useful for our analysis.

Data from the AWS at Das, Malniu and Cadí Nord are in 30-minute averages; data from Martinet and La Molina are 10-minute averaged values and data from Santa Llocaia are hourly average values. To standardize the results of this study, hourly averages from all the variables have been calculated and used. All data series have some blanks that were not considered in the data analysis. In total, there were less than 2% blanks at most of the stations, which was not a concern.

b. Pressure pattern

The mean sea-level pressure of the area including the Pyrenees for each day is used to inspect if the cold-air pool is related to a particular weather type. For the study period, the daily mean sea-level pressure of 0000 UTC is obtained from the ERA-Interim reanalysis covering all Europe with a horizontal resolution of approximately 0.7º (Dee

http://mc.manuscriptcentral.com/joc

et al., 2011). These data are used in the Jenkinson and Collison (1977) synoptic classification to obtain the different types of pressure patterns and have been used in the area by Spellman (2000) for Spain and by Grimalt *et al.* (2013) for the western Mediterranean. Furthermore, a principal component analysis (PCA) is applied to these mean sea-level pressure fields, as Peña *et al.* (2011) did for strong wind events in Catalonia, to identify the main atmospheric patterns related to the occurrence of a CAP in the Cerdanya Valley.

c. Land surface temperatures from MODIS

Land surface temperatures (LSTs) estimated from satellites are a useful validation tool for models, especially when meteorological conditions are dominated by local circulations (cf. Jiménez *et al.*, 2008). In this study, 4 or 5 available images per day from the MODerate resolution Imaging Spectroradiometer (MODIS: Salomonson *et al.*, 1989), on board of the polar Terra and Aqua satellites, provide estimations of LST for the area of interest at an approximate nominal horizontal resolution of 1 km x 1 km, for viewing angle observations close to nadir. LST is calculated using the generalized split-window method, which performs corrections for atmospheric effects based on the differential absorption in the adjacent infrared bands and requires land surface emissivity as an input (Jiménez *et al.*, 2015; Wan and Dozier, 1996).

2.3 Mesoscale MesoNH model

The mesoscale MesoNH model (Lafore *et al.*, 1998) is run to obtain supplementary information on the main governing processes, being conscious of the limitations of the use of a numerical model. Using a setup such as the one used for similar previous

Peer Review Only

studies on complex terrains, especially those in the Pyrenees (Jiménez and Cuxart, 2014) or the surrounding areas (Cuxart *et al.*, 2012), the model outputs are analyzed by always taking into account their correspondence to the available observations previously described.

The simulated period runs from 30/09/2011 at 1200 UTC to 02/10/2011 at 1200 UTC, to allow the model to develop nocturnal circulations after the initial spin-up. The run is initialized using an analysis from the European Centre for Medium-Range Weather Forecasts (ECMWF) and the lateral boundary conditions are refreshed every 6 hours.

Domain 1 (Figure 1a), with a horizontal resolution of 2 km x 2 km, is wide enough to cover a good part of the Pyrenees mountain range, the Mediterranean coast of Catalonia and an area of intermediate altitude in order to get a proper representation of air circulation and avoid problems with the lateral boundary conditions, as suggested by Warner *et al.* (1997). Domain 2 (Figure 1a and Figure 1b), with a horizontal resolution of 400 m x 400 m, includes the Cerdanya Valley and the immediate surrounding areas. This configuration is suitable for a high-resolution mesoscale simulation over complex terrain (Cuxart, 2015). The vertical resolution is fine close to the surface (3 m), and it becomes coarser as the height increases in order to have a better characterization of the physical processes at the lower levels (Jiménez *et al.*, 2008).

3. STATISTICAL STUDY

3.1 Daily cycle of temperature and wind

The analysis of the four-year period of study for the six AWSs provides information on

http://mc.manuscriptcentral.com/joc

the basic characteristics of the Cerdanya Valley climate. Table I summarizes for each station and season of the year the average values for some thermal and dynamical relevant parameters, namely, the mean maxima and minima temperatures, the thermal amplitude, the mean nocturnal cooling rate for 6 hours after sunset and the mean wind direction between 1000 and 1600 UTC for the daytime and between 0000 and 0400 UTC for the nighttime. The standard deviation of the series of mean daily values is provided in parentheses.

It is interesting to note that the largest daily temperature ranges are found at the bottom of the valley, at Das and Martinet, followed by Santa Llocaia, which is located at the high part of the inclined valley floor, and by La Molina; the smallest thermal amplitudes are found at the AWSs with altitudes above 2000 m asl, such as Malniu and Cadí Nord. In Das, the lowest minimal temperatures are found, lower than in the high mountain AWSs, statistically demonstrating the existence of CAP in Cerdanya Valley without performing any filtering of the ensemble of the data. The nocturnal cooling rate is also very large at Das and Martinet, with average cooling rates between 0.73 and 0.95 ºC h^{-1}, with the strongest cooling rate in the summer, when the surface is drier. At night, in the more ventilated stations in Santa Llocaia and La Molina the cooling rate is approximately 0.3 ºC h^{-1}, and the upper mountain stations have very slow cooling rates, never reaching 0.2 ºC h^{-1} on average, which is probably linked to the general radiative cooling of the atmosphere at those levels.

The nocturnal mean wind direction at night shows little variation for a given season and AWS, at Das blowing from E, at Martinet from N and at Santa Llocaia from ENE to ESE, which are the slope directions of the main topographical features at their surroundings (valley slope, La Llosa tributary and the slopes of the Puigmal range,

Peer Review Only

respectively). The station at La Molina indicates a downslope flow (locally SSE), whereas the upper mountain stations at Cadi Nord and Malniu, show a prevalence of a W flow all seasons of the year. The daytime wind is much more variable in direction, but it still shows up-valley flow at the Cerdanya Valley bottom (Das, Santa Llocaia and Martinet), SW and W flow at the upper levels on the southern side (La Molina and Cadí Nord, respectively), whereas at Malniu, on the sunny northern side, the station indicates upslope flows from the S in the warm seasons.

3.2 Cold-air pools

The Cerdanya CAP is of intermediate size, representative of many large valleys in mountainous systems. It is large enough to host an internal flow complexity but rarely shows persistent multiday events, as occurs more often for wider basins. The Cerdanya is a 35-km-long valley and a few km wide at the bottom. The valley floor level decreases in absolute height from 1300 to 900 m asl. The Cerdanya CAP is essentially linked to the valley narrowing at the lower end past Martinet, which does not allow cold air to flow down-valley at low levels as it otherwise would. As simulations indicate, the widening of the Martinet pass at upper heights allows the nocturnal valley jet to flow down-valley further, along the Segre valley past Cerdanya. Therefore, above the CAP, there is a well-defined along-valley flow regime, during both daytime and nighttime, inducing a relatively well-mixed layer, some hundreds of meters deep, in the upper part of the valley atmosphere. The focus of this study is on this strongly stratified layer close to the ground in the CAP, and the layer above it will be where most of the top-bottom mixing events into the CAP may originate.

Peer Review Only

http://mc.manuscriptcentral.com/joc

As simulations and LST from satellite will show, Santa Llocaia is usually near the external margin of the CAP at the end of the night. On the other hand, Das has the lowest minimal temperatures of the three stations at the floor of the valley. These two stations are used to inspect the frequency, duration and maximum strength of the CAP temperature inversion, assuming that the inversion lasts at least 2 hours. A difference of 3 °C is required between the two stations to ascertain that a CAP occurs, as noted by other studies such as Iijima and Shinoda (2000) that recommend 1.33 °C/ 100 m, a rate similar to the one used here. Based on this criterion, it may be concluded that 854 daily cold-air pools were formed in the Cerdanya Valley during the four years analyzed (58.5% of the nights, 7628 h), a similar proportion to the one found in Japan by Iijima and Shinoda (2000), which was 56% of nights with CAP in a subalpine hollow.

Table II provides more details about monthly means and standard deviations and Figure 2 demonstrates the distributions of wind at both stations for CAP nights. A CAP presence is shown on 45.0% of the nights in June and 80.6% in December. In approximately 4.8% of these nights, the temperature difference between Das and Santa Llocaia was larger than -10.0 °C, on 69.9% of the nights larger than -5.0 °C, while the maximum difference was -13.1 °C on the night of 4 to 5 January 2013. CAPs persist usually more than 5 hours and lasted 12 or 13 hours in December and January. When a CAP is present, the wind speed is very low (approximately 65% of the time below 2 m s^{-1} and 90% of the time below 3 m s^{-1}) at Das (Figure 2a) and at Santa Llocaia (not shown). Due to the topographical configuration, a CAP can be formed when there are significant winds at higher levels, as is the case for the station at Cadí Nord, with only 16.6% of the nights with wind speeds below 2 m s^{-1} during CAP episodes. Significant winds just above the surface of a thermal inversion can affect the evolution of the

Peer Review Only

inversion, for instance, when a down-valley wind is blowing over it, but this phenomenon cannot be explored with the AWSs used in this study. Numerical modeling and vertical observations are necessary to characterize this issue further. It is observed that, for Das, the flow is mainly coming down-valley (E) and from the La Molina tributary valley (SE) (Figure 2b). However, in the highest part of the valley floor, in the wide area of Santa Llocaia, the wind direction ranges from E (upper part of the Cerdanya Valley) to S (Puigmal subrange) (Figure 2c).

All days of the 4-year study period were classified according to the pressure pattern types of the Jenkinson and Collison classification. Then, CAP nights were classified into the different synoptic pressure pattern types. Only 19.1% of nights are related to a purely anticyclonic pattern, and 24.6% of nights are associated with purely cyclonic patterns, while most of the other cases have mixed patterns. This result is consistent with the expectation that tall and steep topography decouples the lower circulations close to the surface from the general flow at approximately 1500 m above the mountain ranges. Furthermore, other studies have shown that there is not necessarily a need for an anticyclone to develop a CAP, even in flat terrain, as was the case studied by Pepin *et al.* (2009) for Finland. However, the next subsection describes that the strongest CAP events are effectively associated with anticyclonic conditions.

3.3 Selection of stable nights

a. Selection method

Peer Review Only

We applied the method of Martinez *et al.* (2008) to select the best defined, most stable CAP cases. That study applies a filter to an AWS dataset to select the stably stratified nights that occurred over a lower wide basin such as the Ebro River valley floor.

In total, three parameters related to the most common variables measured in an AWS were defined:

$$Q_d = \frac{Q_t - Q_e}{Q_t} \quad (1)$$

$$iHUM = \frac{HR_d - HR_s}{HR_d} \quad (2)$$

$$\overline{V_n} = \frac{1}{N}\sum_{i=1}^{N} v_i \quad (3)$$

The insolation deficit index (Q_d) allows the selection of those cases in which the observed average daily insolation (Q_e) is closer to the theoretical value at the top of the atmosphere (Q_t) and thus filters days under cloudy conditions. This method assumes that the cloudiness observed during daylight is similar to the following night.

The humidity cycle index (*iHUM*) allows the identification of those cases with a large contrast relative humidity between day and night, since RH_d and RH_s represent the mean relative humidity for the entire day and for daylight only, respectively.

The mean nocturnal wind speed ($\overline{V_n}$) calculated between sunset and sunrise classifies the observed wind intensity during the night. All nights with a mean speed below 2 m s^{-1}

Peer Review Only

are selected to avoid cases under the influence of important synoptic or mesoscale pressure gradients, which produce moderate wind speeds near the surface.

Martinez *et al.* (2008) define the corresponding thresholds for each parameter after an accurate inspection of their values during several single selected cases. Thus, these thresholds are site-dependent and they have been modified for the current case following a similar procedure, i.e., after the inspection of some very good CAP cases occurred within the Cerdanya Valley. As a result, the nights considered stably stratified over the valley floor are those that fulfil the following conditions at the Das AWS:

$$Q_d \leq 0.3; \quad iHUM \geq 0.28; \quad \overline{V_n} \leq 2\ m\ s^{-1} \tag{4}$$

The application of these filtering criteria allows for the selection of those nights with weak winds, preceded by a day with little cloudiness and a dry atmosphere compared with the nocturnal values. Furthermore, the selection is only made on the subset of nights between March and October (980 days in 4 years), since in this study, we focus on conditions without snow in the lower part of the valley; the analysis of cases with snow will be reported in a later study. The application of the filter detects 163 low-cloud non-windy nights (17%) for which the CAP quantities described above will be calculated. If a principal component analysis (PCA) is applied on this selected subset, then most of the patterns related to CAPs correspond to a kind of anticyclonic conditions around the valley. The three most representative patterns, including 62.6% of the selected nights, show a Central European anticyclone, sometimes with light NE cold advection over the Pyrenees; the fourth pattern (16.6%) shows a barometric swamp; and the last three patterns (20.8%) are associated with anticyclones to the north or the west.

Peer Review Only

b. *The daily cycle*

The daily cycle of the meteorological variables logically depends on the month or season of the year, but the shape of the cycles of the six AWSs in each month or season is very similar. Therefore, all the data have been used together to draw the annual mean daily cycle of the selected stable nights. For temperature (Figure 3a), a large daily range appears for the two stations at the lowest elevations (Das and Martinet), the cycle loses definition as it goes to AWS located higher in the valley, and a well-defined thermal inversion is evident in the Figure.

The cooling rate from sunset (Figure 3b) is highest at the valley bottom, with very similar sustained evolutions for Das and Martinet, which are inside the CAP. Stations in the narrow valley of La Molina or at the Puigmal foothills in Santa Llocaia have slower rates, essentially constant for 4 hours after the sunset. Instead, for the AWSs at upper levels in the valley above the cooling rate are lower and restricted to the first hours of the night. Comparing these evolutions to those described in Martinez *et al.* (2008), we see that the evolutions of Santa Llocaia and La Molina, which are well ventilated and usually under low-level jets (LLJ) and weak stability (according to the available simulations, such as the one described below), are similar to the one in Gimenells at the Ebro Valley floor, also usually under basin-scale LLJs under anticyclonic conditions.

An integrated way of comparing the different stations is by means of the probability density function (PDF) of the differences between the minimum temperatures. Figure 3c shows the distributions for the selected stable nights between Das, Santa Llocaia and the three mountain AWSs. Between the center of the CAP (Das) and its outer limit (Santa Llocaia), the PDF is almost Gaussian, narrow and centered around -5 °C, indicating

Peer Review Only

similar behavior and colder air at the bottom. Instead, the differences with the upper AWSs are more widely spread with longer tails, indicating less correlation, with smaller mean differences since the upper stations are colder, because they are at higher altitudes.

Inspection of the evolution of the mean wind direction (Figure 3d) displays very clear changes in the morning and evening transitions at the valley floor, changing respectively to up-valley wind from the SSW and to down-valley wind from the NNE. The stations at the slopes also change, each following the local slope. The station of Cadi Nord, at the top of the southern mountain range, has a prevailing westerly wind.

4. MODEL RESULTS

4.1. Selection of the case.

Two days have been chosen from the selected stable days to better investigate the phenomenon through a high-resolution mesoscale simulation. This period starts on 30/09/2011 at 1200UTC, and ends on 02/10/2011 at 1200 UTC. Astronomical sunset and sunrise occurred at 1732 and 0555 UTC in Das, respectively.

These days display a behavior (Figure 4) very similar to the general characteristics shown in Figure 3, with the temperature being somewhat lower than the annual average but with very large thermal amplitudes (23ºC) at Das and Martinet, and a minimum temperature of 0 ºC at Das and 2.5 ºC at Martinet.

Similarly, the shapes of the other variables and AWSs are comparable with the average cycles (not shown). Down in the valley, the wind speed attains its maximum in the

http://mc.manuscriptcentral.com/joc
Peer Review Only

afternoon, only some hours later than the maximum temperature, near sunset, and at night, the wind is very weak. Higher in the valley, the evolution of the wind is more location dependent, and at Cadi-Nord the wind does not reflect the diurnal cycle.

This section analyses the results provided by the simulation performed with the MesoNH model. Our aim is to determine if the model is able to simulate the CAP, and, if so, to describe some aspects of the CAP development, estimating the occupied area and its depth, and classify the wind regimes in the valley, as viewed from the simulation.

Peer Review Only

4.2 Verification

When the AWS measurements are compared to the model results for the nearest grid point, it is shown that the mesoscale model predicts a behavior very similar to the one observed for all the variables; however, it is unable to retrieve the proper maximum and minimum temperature values (Figure 4). At the bottom of the valley, inside the CAP, the model overestimates the minimum temperature by 6ºC. Instead, in more ventilated areas, such as Santa Llocaia, there is not discrepancy. The difficulties of models in quantitatively characterizing, in a correct manner, very stable surface layers are known, even if many times, the qualitative description is very similar to reality, such as the case here or other recent studies on complex terrain, such as Jiménez and Cuxart (2014) and Pagès et al. (2017).

The adequate qualitative correlations can be seen when comparing the structures of the simulated and the satellite LST fields, which are very much alike, since they have comparable resolutions. At nighttime (Figure 5a), the LST field from satellites indicates

http://mc.manuscriptcentral.com/joc

that the coldest areas are at the top of the mountain ranges and at the bottom of the Cerdanya Valley. The differences between the satellite LST and the model are not large in the CAP region (not shown) compared to the difference between the modeled and observed air temperatures at 1.5 m agl. The closeness in values of LST may be explained by the action of the surface scheme, which partially corrects the warm bias of the surface layer in the model. This good agreement is confirmed for most of the MODIS fields, as seen in Figure 5b, where the mean MODIS LST always is within the uncertainty of the model average.

4.3 Area and depth of the CAP

Two sub-CAPs appear in the bottom of the valley, due to the topographic separation in between the areas surrounding Martinet and Das (see Figure 1b), the latter being colder than the former, as indicated by the observational study (see Figure 5a).

The time-space variations of the model LST and temperature at 1.5 m (T1.5) are used to locate and measure the cold-air pool. Martínez *et al.* (2010) proposed a temperature decomposition similar to that in Lundquist *et al.* (2008), where the temperature $T(x,y,t)$ is split into three terms

$$T(x,y,t) = \bar{T}(x,y) + \bar{T}'(t) + \tilde{T}(x,y,t) \qquad (5)$$

Here $\bar{T}(x,y)$ is the mean nocturnal temperature for the whole area, using values between 1730 and 0530 UTC; $\overline{T'}(t)$ is the time series of the deviation of the instantaneous area-averaged value with respect to the mean; and $\tilde{T}(x,y,t)$ is an

http://mc.manuscriptcentral.com/joc
Peer Review Only

instantaneous 3D field containing the rest of the field, the local spatial deviation that changes through time. The decomposition equation has been applied to model outputs every 30 minutes for the two nights, which behave very similarly, and only the night between 1 and 2 October is discussed here, and some results are shown in Figure 6.

The mean nocturnal temperature $\bar{T}(x,y)$ field (Figure 6a) shows the coldest and warmest areas; the center of the bottom of the valley being colder than its immediate surroundings. The evolution of the basin-averaged deviation $\bar{T}'(t)$ from the mean nocturnal temperature is shown in Figure 6b. It shows the evolution of $\overline{LST'}(t)$ and $\bar{T}'_{1.5}(t)$, and $\overline{LST'}(t)$ decreases faster than $\bar{T}'_{1.5}(t)$, especially at the beginning of the night, with the ground temperature deviation becoming lower than the value of the adjacent air from 2100 UTC on, but its total cooling is always larger (8 °C) than the 1.5 m temperature (3 °C). Contrary to the case of Martínez *et al.* (2010), the present area includes steep slopes and altitudinal variations in temperatures, with a different interpretation, but it is still useful to locate the CAP area in a deep valley and its evolution.

Comparing the field $T(x,y,t)$ at any time with its values at the beginning of the night t_0 (defined as the last registered data before sunset, 1730 UTC for this simulation), the difference between these values can be defined as:

$$T(x,y,t) - T(x,y,t_0) = [\bar{T}'(t) - \bar{T}'(t_0)] + [\tilde{T}(x,y,t) - \tilde{T}(x,y,t_0)] \quad (6)$$

or

$$\Delta T(x,y,t) = \Delta\bar{T}'(t) + \Delta\tilde{T}(x,y,t) \quad (7)$$

http://mc.manuscriptcentral.com/joc

where the first term on the right side illustrates the mean night cooling of the basin from sunset until *t*, which could be easily calculated from Figure 6b, and the second describes the existence or not of anomalies in different places, such as sites with warmer or cooler temperature anomalies than the field average. As cooler temperature anomalies could be related to the existence of a CAP (Lundquist *et al.*, 2008), we will use this second term to study the CAP evolution.

Figure 6c presents the area in domain 2 with $\Delta\tilde{T}(x, y, t) \leq -1.0\,°C$, throughout the entire night, showing the points with a surface nocturnal cooling at least 1 °C greater than the mean cooling of the basin; consequently, according to equation 7, the domain has cooled more than 9 °C (8 °C + 1 °C) during the entire night. If we consider this value as a threshold to predict the CAP location, then we see a vast CAP area in the main valley, and many patches were scattered around the domain corresponding to some small and deep valleys in the mountain ranges on both sides of the main valley.

Focusing on the principal valley, the region of interest that is analyzed is defined as the area within the box shown in Figure 6c with a topographic elevation of less than 1500 m; its surface area is approximately 362 km^2. In Figure 7a the blue line indicates the growing rate of the CAP from sunset, when it begins to build up at the bottom of the valley at 1830 UTC, spreading quickly until it covers almost 50% of the valley at 2000 UTC and 80% at 0030 UTC, and later extending slowly to cover up to 86% by the end of the night. Other lines changing the threshold indicate similar behavior but with less extension as $|\Delta\tilde{T}(x, y, t)|$ increases. Approximately 50% of the valley cools 4 °C more than the mean cooling of the basin. The two subCAPs connect at approximately 2000

http://mc.manuscriptcentral.com/joc
Peer Review Only

UTC once their depth becomes larger than the height of the topographic obstacle separating them (not shown).

Simulated results show that the vertical profile of the potential temperature inside the CAP has a strong stably stratified layer close to the ground followed by a less stable one aloft (see Figures 7c and 7d). To estimate the temporal evolution of these layers, Figure 7b shows the mean altitude of the grid points in the vertical cross-section of the CVL-1 (Figure 1b) at two different reference temperatures. One value is representative of the surface inversion (292 K), while the other value corresponds to the layer above it. The lowest layer increases its altitude as the night advances, with a final mean value of 1180 m asl for the threshold 292 K, corresponding to a maximum depth of 130 m in the deepest points of the valley and a very strong mean vertical potential temperature gradient of 10K/100m in the CVL-1 axis. Instead, the reference value for the upper layer increases progressively until past midnight, indicating a general cooling of the layer, which will be described in subsection 4.5. After this time, the upper layer remains steady for the rest of the night. The fact that Das is always inside the strong stable layer and Santa Llocaia is often above it may explain the good performance of the temperature difference between them as indicator of the CAP.

4.4 Down-valley and down-slope circulations

At nighttime, the valley topography completely conditions the circulation in the valley when a CAP is formed. If different tributary valleys or mountain slopes produce some drainage currents, they may converge over the center of the complex valley and join each other to generate a deeper drainage current, flowing along the main valley

http://mc.manuscriptcentral.com/joc

(Gudiksen *et al.*, 1992; Neff and King, 1989). Figure 8 shows the mature flow structure after midnight; this structure is very similar for the two simulated nights and the discussion will be focused on the second night (between 1 and 2 October).

The characteristic nocturnal circulations in the CAP, including Das along the main valley axis, are indicated in Figure 8b at 0030 UTC. A moderately strong synoptic wind (up to 7 m s^{-1}, not shown) from the N-NE sectors is confined to heights above 2000 m asl, while the wind below takes much lower speeds. A weak down-valley wind forms close to the surface, where thermal stratification is stronger, with maximum wind speeds of 3 m s^{-1} that appear intermittently over different parts of the main valley axis along the night. An intermediate layer with very low winds (~1 m s^{-1}) from SE separates the upper general wind from the thermally-driven flows close to the surface. The interaction with the main tributaries (La Molina (CVL-M) and Querol (CVL-Q), see Figure 1b) can be seen in Figure 9a and 9b, where the temporal evolution of the amount of down-valley flows below 200 m agl and their speed are shown. The main valley (CVL-1) progressively builds up the down-valley circulation (wind direction ranging between CVL-1 direction (65º) ± 60º), reaching more than 60% shortly after sunset and near 95% at 2230 UTC and experiencing variations later in the night; the averaged wind speeds remaining low (below 2 m s^{-1}).

The Querol tributary (CVL-Q) shows down-valley circulation (wind direction ranging between 310º ± 60º) reaching up to 90% until 1.5 h after sunset, and then it varies between 20% and 80% during the rest of the night, indicating that this structure especially contributes to the accumulation of air in the main valley at the beginning of the night. The behavior of the La Molina tributary in S is different. First, it has a down-

Peer Review Only

http://mc.manuscriptcentral.com/joc

valley flow (wind direction ranging between 112º ± 60º) during the late afternoon due to the mesoscale pumping of the heated southern side of the mountains that generates S flow most of the time during daytime. This circulation stops shortly after sunset, and the true nocturnal down-valley flows start 1.5 hours after sunset, which stay blowing all night with values at approximately 80% until after sunrise. Between 0100 and 0330 UTC, the wind becomes stronger and modifies the down-valley circulation in the main valley, as it is shown in Figure 9a (CVL-1). Still, observational information would be needed to determine if the air from the tributaries weakens or strengthens the CAP in the Cerdanya Valley, as evaluated by Zangl (2005) for an alpine valley system.

4.5 The heat budget

Figure 10a shows the most significant factors that change the amount of heat in the CAP, according to the model. The time evolution indicates that in the surface layer before 2130 UTC, only dissipation warms the CAP, whereas total advection, vertical turbulence and radiative divergences contribute to a very significant cooling tendency. Later, total advection becomes a warming factor, and the cooling rate diminishes to half the previous value during the rest of the night. Advection and radiation show slowly varying evolutions, whereas turbulence mixing seems to drive the short-term changes.

The mean vertical profile of the heat budget for the period 0000-0400 UTC (Figure 10b) shows that in the surface layer (up to 10 m agl), where the strongest stable stratification takes place, the advection warms. This process is most likely driven by subsidence since the vertical wind is negative (not shown), pushing the warmer air downward. Instead, the cold advection aloft may be explained by the horizontal transport of colder air

Peer Review Only

originated over the slopes at similar heights that cannot penetrate into the underlying stably stratified layer. This mechanism could bring an eventual upward adiabatic motion (consistent with mass conservation), favoring the air cooling and deepening the CAP, as is suggested by Kiefer and Zhong (2011) for the meteor crater in Arizona. Turbulence is important in the surface layer and areas above it can be neglected, according to the model outputs.

5. Concluding summary

The Cerdanya Valley in the Pyrenees has a frequent occurrence of cold pooling in the bottom of valley, as the statistical analysis presented in this work has shown. Major occurrences of valley-wide cold pools, as detected between the lower and higher parts of the valley floor, occur in long winter, stably stratified nights. However, this feature is frequently observed during the whole year, and it is not necessarily related with the presence of high pressures over the region. The particular topography of the valley probably protects its lower areas from the general winds not blowing along the valley axis, allowing a cold-air pool to develop even in the presence of significant synoptic pressure gradients.

The period of the year between March and October was selected for identifying the characteristics of the cold pool without snow in the bottom of the valley, leaving the study of this particular topic to a further experimental study. A selection of clear days and weak general winds was made, which the PCA indicates normally occur in high synoptic pressure conditions. The average daily cycles of the main meteorological

Peer Review Only

variables for this selection do not depart much from the ensemble average, indicating the prevalence of this feature in the area. Very wide 24-h oscillations occur for the temperature at the bottom of the valley, whereas the upper parts show a much weaker sign. Wind blows downslope late afternoon and early evening, having down-valley flows during the night. Upslope and up-valley flows are established during the day.

In the early autumn of 2011, the structure and evolution of the cold-air pool was studied for a period of 2 days that, which is very close to CAP average behavior. A simulation with a horizontal resolution of 400 m is performed over the valley and the surrounding mountains and qualitatively compares well with the in situ observations and the LST as provided by MODIS on board Terra and Aqua satellites. Simulations indicate that the cold-air pool manages to extend to 80% of the bottom of the valley in a few hours, combined with a slow growth of the cold pool depth. Furthermore, the turning of the wind to down-valley along the main axis occurs from before to two to three hours after sunset, and the wind blows in the same direction until well after sunrise. The main tributaries bring air to the CAP at different rates and presumably results in its shape and strength varying, accordingly. The inspection of the energy budget at the center of the valley indicates that the divergence of the radiative and turbulent heat fluxes are the main cooling mechanisms, the latter in the lower tens of meters agl. Advection cools, probably as colder air blows over the site, except in the surface layer when the CAP is already set, where downward vertical velocity produces warm advection.

These modeled mechanisms should be confirmed or rejected by means of experimental work on site, especially for the low values of elevated turbulence in the down-valley flows, since mesoscale models tend to underestimate the LLJ-related turbulent mixing.

Peer Review Only

Acknowledgements

This work was partially funded by grants from the Spanish government CGL2015-65627-C3-1-R (AEI/FEDER, UE). Data from the automatic weather stations have been provided by Meteocat, AEMET and MétéoFrance. ECMWF and AEMET are thanked for the access to computing time and the MesoNH team in MétéoFrance and Laboratoire d'Aérologie for their suport.

Peer Review Only

References

Clements CB, Whiteman CD, Horel JD. 2003. Cold-Air-Pool Structure and Evolution in a Mountain Basin: Peter Sinks, Utah. *Journal of Applied Meteorology* **42**: 752–768. DOI: 10.1175/1520-0450(2003)042<0752:CSAEIA>2.0.CO;2.

Cuxart J. 2008. Nocturnal basin low-level jets: an integrated study. *Acta Geophysica*. Versita **56**(1): 100–113. DOI: 10.2478/s11600-007-0042-2.

Cuxart J. 2015. When Can a High-Resolution Simulation Over Complex Terrain be Called LES? *Frontiers in Earth Science*. Frontiers **3**: 87. DOI: 10.3389/feart.2015.00087.

Cuxart J, Cunillera J, Jiménez MA, Martínez D, Molinos F, Palau JL. 2012. Study of Mesobeta Basin Flows by Remote Sensing. *Boundary-Layer Meteorology*. Springer Netherlands **143**(1): 143–158. DOI: 10.1007/s10546-011-9655-8.

Cuxart J, Holtslag a. a. M, Beare RJ, Bazile E, Beljaars A, Cheng A, Conangla L, Ek M, Freedman F, Hamdi R, Kerstein A, Kitagawa H, Lenderink G, Lewellen D, Mailhot J, Mauritsen T, Perov V, Schayes G, Steeneveld G-J, Svensson G, Taylor P, Weng W, Wunsch S, Xu K-M. 2006. Single-column model intercomparison for a stably stratified atmospheric boundary layer. *Boundary-Layer Meteorology* **118**(2): 273–303. DOI: 10.1007/s10546-005-3780-1.

Dee DP, Uppala SM, Simmons AJ, Berrisford P, Poli P, Kobayashi S, Andrae U, Balmaseda MA, Balsamo G, Bauer P, Bechtold P, Beljaars ACM, van de Berg L, Bidlot J, Bormann N, Delsol C, Dragani R, Fuentes M, Geer AJ, Haimberger L, Healy SB,

For Peer Review Only

http://mc.manuscriptcentral.com/joc

Hersbach H, Hólm E V., Isaksen L, Kållberg P, Köhler M, Matricardi M, McNally AP, Monge-Sanz BM, Morcrette J-J, Park B-K, Peubey C, de Rosnay P, Tavolato C, Thépaut J-N, Vitart F. 2011. The ERA-Interim reanalysis: configuration and performance of the data assimilation system. *Quarterly Journal of the Royal Meteorological Society*. John Wiley & Sons, Ltd. **137**(656): 553–597. DOI: 10.1002/qj.828.

Grimalt M, Tomàs M, Alomar G, Martin-Vide J, Moreno-García MC. 2013. Determination of the Jenkinson and Collison's weather types for the western Mediterranean basin over the 1948-2009 period. Temporal analysis. *Atmósfera* **26**(1): 75–94. DOI: 10.1016/S0187-6236(13)71063-4.

Gudiksen PH, Leone JM, King CW, Ruffieux D, Neff WD. 1992. Measurements and Modeling of the Effects of Ambient Meteorology on Nocturnal Drainage Flows. *Journal of Applied Meteorology* **31**(9): 1023–1032. DOI: 10.1175/1520-0450(1992)031<1023:MAMOTE>2.0.CO;2.

Gustavsson T, Karlsson M, Bogren J, Lindqvist S. 1998. Development of Temperature Patterns during Clear Nights. *Journal of Applied Meteorology* **37**(6): 559–571. DOI: 10.1175/1520-0450(1998)037<0559:DOTPDC>2.0.CO;2.

Holtslag AAM, Svensson G, Baas P, Basu S, Beare B, Beljaars ACM, Bosveld FC, Cuxart J, Lindvall J, Steeneveld GJ, Tjernström M, Van De Wiel BJH, Holtslag AAM, Svensson G, Baas P, Basu S, Beare B, Beljaars ACM, Bosveld FC, Cuxart J, Lindvall J, Steeneveld GJ, Tjernström M, Wiel BJH Van De. 2013. Stable Atmospheric Boundary Layers and Diurnal Cycles: Challenges for Weather and Climate Models. *Bulletin of the American Meteorological Society*. American Meteorological Society **94**(11): 1691–

Peer Review Only

1706. DOI: 10.1175/BAMS-D-11-00187.1.

Iijima Y, Shinoda M. 2000. Seasonal changes in the cold-air pool formation in a subalpine hollow, central Japan. *International Journal of Climatology* **20**(12): 1471–1483. DOI: 10.1002/1097-0088(200010)20:12<1471::AID-JOC554>3.0.CO;2-6.

Jenkinson A, Collison F. 1977. *An initial climatology of gales over the North Sea. Synoptic climatology branch memorandum*. Meteorological Office: Barcknell.

Jiménez MA, Cuxart J. 2014. A study of the nocturnal flows generated in the north side of the Pyrenees. *Atmospheric Research* **145**: 244–254. DOI: 10.1016/j.atmosres.2014.04.010.

Jiménez MA, Mira A, Cuxart J, Luque A, Alonso S, Guijarro JA. 2008. Verification of a Clear-Sky Mesoscale Simulation Using Satellite-Derived Surface Temperatures. *Monthly Weather Review* **136**(12): 5148–5161. DOI: 10.1175/2008MWR2461.1.

Jiménez MA, Ruiz A, Cuxart J. 2015. Estimation of cold pool areas and chilling hours through satellite-derived surface temperatures. *Agricultural and Forest Meteorology*. Elsevier B.V. **207**: 58–68. DOI: 10.1016/j.agrformet.2015.03.017.

Kiefer MT, Zhong S. 2011. An idealized modeling study of nocturnal cooling processes inside a small enclosed basin. *Journal of Geophysical Research* **116**(D20): D20127. DOI: 10.1029/2011JD016119.

Lafore JP, Stein J, Asencio N, Bougeault P, Ducrocq V, Duron J, Fischer C, Héreil P, Mascart P, Masson V, Pinty JP, Redelsperger JL, Richard E, Vilà-Guerau de Arellano J. 1998. The Meso-NH Atmospheric Simulation System. Part I: adiabatic formulation and control simulations. *Annales Geophysicae*. Springer-Verlag **16**(1): 90–109. DOI:

Peer Review Only

10.1007/s00585-997-0090-6.

Lareau NP, Horel JD. 2015. Dynamically Induced Displacements of a Persistent Cold-Air Pool. *Boundary-Layer Meteorology* **154**(2): 291–316. DOI: 10.1007/s10546-014-9968-5.

Lundquist JD, Pepin N, Rochford C. 2008. Automated algorithm for mapping regions of cold-air pooling in complex terrain. *Journal of Geophysical Research Atmospheres* **113**(22). DOI: 10.1029/2008JD009879.

Martinez D, Cuxart J, Cunillera J. 2008. Conditioned climatology for stably stratified nights in the Lleida area. *Tethys, Journal of Weather and Climate of the Western Mediterranean* **5**: 13–24. DOI: 10.3369/tethys.2008.5.02.

Martínez D, Jiménez MA, Cuxart J, Mahrt L. 2010. Heterogeneous Nocturnal Cooling in a Large Basin Under Very Stable Conditions. *Boundary-Layer Meteorology* **137**(1): 97–113. DOI: 10.1007/s10546-010-9522-z.

Neff WD, King CW. 1989. The Accumulation and Pooling of Drainage Flows in a Large Basin. *Journal of Applied Meteorology* **28**(6): 518–529. DOI: 10.1175/1520-0450(1989)028<0518:TAAPOD>2.0.CO;2.

Pagès M, Miró JR. 2010. Determining temperature lapse rates over mountain slopes using vertically weighted regression: a case study from the Pyrenees. *Meteorological Applications*. John Wiley & Sons, Ltd. **17**(1): 53–63. DOI: 10.1002/met.160.

Pagès M, Pepin N, Miró JR. 2017. Measurement and modelling of temperature cold pools in the Cerdanya valley (Pyrenees), Spain. *Meteorological Applications*. John Wiley & Sons, Ltd **24**(2): 290–302. DOI: 10.1002/met.1630.

Peer Review Only

Peña JC, Aran M, Cunillera J, Amaro J. 2011. Atmospheric circulation patterns associated with strong wind events in Catalonia. *Natural Hazards and Earth System Science*. Copernicus GmbH **11**(1): 145–155. DOI: 10.5194/nhess-11-145-2011.

Pepin NC, Schaefer MK, Riddy LD. 2009. Quantification of the cold - air pool in Kevo Valley , Finnish Lapland. *Weather* – **64**(3). DOI: 10.1002/wea.260.

Salomonson VV, Barnes WL, Maymon PW, Montgomery HE, Ostrow H. 1989. MODIS: advanced facility instrument for studies of the Earth as a system. *IEEE Transactions on Geoscience and Remote Sensing*. IEEE **27**(2): 145–153. DOI: 10.1109/36.20292.

Smith SA, Brown AR, Vosper SB, Murkin PA, Veal AT. 2010. Observations and Simulations of Cold Air Pooling in Valleys. *Boundary-Layer Meteorology*. Springer Netherlands **134**(1): 85–108. DOI: 10.1007/s10546-009-9436-9.

Spellman G. 2000. The application of an objective weather-typing system to the Iberian peninsula. *Weather* **55**(10): 375–385. DOI: 10.1002/j.1477-8696.2000.tb04023.x.

Viterbo P, Beljaars A, Mahfouf J-F, Teixeira J. 1999. The representation of soil moisture freezing and its impact on the stable boundary layer. *Quarterly Journal of the Royal Meteorological Society*. John Wiley & Sons, Ltd **125**(559): 2401–2426. DOI: 10.1002/qj.49712555904.

Vosper SB, Brown AR. 2008. Numerical simulations of sheltering in valleys: The formation of nighttime cold-air pools. *Boundary-Layer Meteorology* **127**(3): 429–448. DOI: 10.1007/s10546-008-9272-3.

Wan Z, Dozier J. 1996. A generalized split-window algorithm for retrieving land-

Peer Review Only

surface temperature from space. *IEEE Transactions on Geoscience and Remote Sensing*. IEEE **34**(4): 892–905. DOI: 10.1109/36.508406.

Warner TT, Peterson RA, Treadon RE. 1997. A Tutorial on Lateral Boundary Conditions as a Basic and Potentially Serious Limitation to Regional Numerical Weather Prediction. *Bulletin of the American Meteorological Society* **78**(11): 2599–2617. DOI: 10.1175/1520-0477(1997)078<2599:ATOLBC>2.0.CO;2.

Young JS, Whiteman CD. 2015. Laser ceilometer investigation of persistent wintertime cold-air pools in Utah's Salt Lake Valley. *Journal of Applied Meteorology and Climatology* **54**(4): 752–765. DOI: 10.1175/JAMC-D-14-0115.1.

Yu L, Zhong S, Bian X. 2017. Multi-day valley cold-air pools in the western United States as derived from NARR. *International Journal of Climatology* **37**(5): 2466–2476. DOI: 10.1002/joc.4858.

Zangl G. 2005. Dynamical Aspects of Wintertime Cold-Air Pools in an Alpine Valley System. *Monthly Weather Review* **133**(1985): 2721–2740. DOI: 10.1175/MWR2996.1.

Zardi D, Whiteman CD. 2013. Diurnal Mountain Wind Systems. Springer Netherlands, 35–119. DOI: 10.1007/978-94-007-4098-3_2.

Zhong SY, Whiteman CD, Bian XD, Shaw WJ, Hubbe JM. 2001. Meterological processes affecting the evolution of a wintertime cold air pool in the Columbia Basin. *Monthly Weather Review* **129**(10): 2600–2613. DOI: 10.1175/1520-0493(2001)129<2600:MPATEO>2.0.CO;2.

Peer Review Only

http://mc.manuscriptcentral.com/joc

Peer Review Only

http://mc.manuscriptcentral.com/joc

TABLES

Table I. Maximum and minimum temperature of the mean daily cycle, thermal amplitude, mean nocturnal cooling rate (for six hours after the sunset) and mean wind direction (between 0000 UTC and 0400 UTC for the nighttime and between 1000 UTC and 1600 UTC for the daytime), in the period from 01/09/2010 to 31/08/2014. Standard deviations are in parentheses.

		Tmax (°C)	Tmin (°C)	TA (°C)	NC (°C/h)	WDnight (°)	WDday (°)
	Win.	9.0 (5.4)	-3.2 (4.4)	12.1	0.73 (0.48)	82.2	29.7
DA	Spr.	17.9 (5.9)	4.2 (4.1)	13.7	0.80 (0.42)	103.8	222.7
1097 m	Sum.	24.2 (4.6)	8.4 (3.1)	15.7	0.95 (0.41)	99.7	232.4
	Aut.	11.7 (6.3)	-0.4 (5.7)	12.0	0.75 (0.45)	84.6	330.2
	Win.	8.1 (5.4)	-0.1 (3.7)	8.2	0.28 (0.26)	76.7	2.3
SL	Spr.	16.6 (5.8)	6.8 (4.2)	9.8	0.36 (0.23)	103.1	201.6
1320 m	Sum.	22.9 (4.7)	11.5 (2.9)	11.4	0.35 (0.22)	116.1	204.6
	Aut.	10.9 (6.1)	3.0 (4.7)	7.8	0.32 (0.24)	105.3	234.6
	Win.	12.1 (5.7)	-2.1 (4.1)	14.2	0.81 (0.42)	8.4	189.8
MR	Spr.	20.8 (6.3)	5.8 (4.2)	14.9	0.81 (0.37)	20.3	258.1
1038 m	Sum.	27.6 (5.0)	10.6 (2.9)	17.0	0.94 (0.37)	31.8	256.3
	Aut.	14.8 (6.2)	1.1 (5.4)	13.7	0.78 (0.35)	35.4	224.2
	Win.	0.6 (5.4)	-3.0 (4.7)	3.6	0.09 (0.24)	325.8	250.4
ML	Spr.	8.3 (5.6)	3.5 (5.0)	4.8	0.14 (0.18)	291.1	185.5
2230 m	Sum.	14.4 (4.1)	9.3 (3.5)	5.2	0.14 (0.18)	280.5	185.9
	Aut.	4.3 (5.9)	1.0 (5.2)	3.3	0.08 (0.23)	309.7	210.9
	Win.	4.4 (4.9)	-1.5 (4.0)	5.9	0.21 (0.24)	193.7	294.9
LM	Spr.	12.3 (5.5)	5.0 (4.7)	7.3	0.32 (0.22)	153.6	225.7
1704 m	Sum.	18.9 (4.1)	10.4 (3.4)	8.4	0.37 (0.23)	151.6	221.5
	Aut.	7.7 (6.0)	2.3 (4.8)	5.4	0.19 (0.25)	164.3	263.3
	Win.	0.2 (4.9)	-2.8 (4.7)	3.1	0.10 (0.22)	239.7	263.9
CN	Spr.	8.6 (5.5)	4.1 (5.1)	4.5	0.15 (0.18)	242.1	275.1
2143 m	Sum.	14.5 (3.9)	9.9 (3.5)	4.6	0.17 (0.21)	244.6	282.9
	Aut.	3.4 (5.7)	1.4 (5.2)	2.0	0.08 (0.23)	245.0	258.0

Peer Review Only

http://mc.manuscriptcentral.com/joc

Table II. Percentage of days with cold-air pool, mean strength (S) and mean duration (D) per month, in the period from 01/09/2010 to 31/08/2014, for the temperature difference criteria between Das and Santa Llocaia (T_{DA} - T_{SL}) ≤ - 3.0 °C.
Standard deviation values are in parentheses.

	T_{DA} - T_{SL} ≤ -3.0 °C				
	% days	S (°C)		D (h)	
Jan.	70.2	-7.4	(2.4)	12.6	(5.1)
Feb.	50.0	-6.7	(2.1)	9.7	(4.3)
Mar.	52.4	-6.1	(1.6)	8.2	(3.1)
Apr.	45.0	-5.8	(1.2)	6.5	(2.7)
May	54.0	-5.4	(1.2)	5.2	(1.9)
Jun.	45.0	-5.5	(1.2)	6.6	(2.1)
Jul.	50.8	-5.3	(1.3)	5.8	(2.3)
Aug.	61.3	-5.7	(1.3)	7.1	(2.8)
Sep	70.8	-6.0	(1.4)	7.8	(2.9)
Oct	65.3	-6.3	(2.0)	9.5	(3.8)
Nov.	55.0	-6.2	(1.9)	10.3	(4.3)
Dec.	80.6	-7.1	(2.1)	13.9	(5.4)

For Peer Review Only

FIGURE LEGEND

Figure 1. (a) Topographic map of the Pyrenees mountain range of northeastern Spain and the South of France. The two domains for the simulations are shown (domain 2 inside domain 1). (b) Topographic map of domain 2, showing AWS locations (DA, SL, MR, ML, LM, CN) and some longitudinal axes used as vertical cross-sections in the simulation (CVL-1, CVL-M, CVL-Q).

Peer Review Only

Figure 2. (a) Bivariate histogram plot of percentage of cold-air pool days and the mean wind speed from sunset to sunrise at Das versus cold-air pool maximum strength. The temperature difference criterion is T_{DA}-T_{SL} ≤ -3 °C. The size and color of the markers indicate the heights of the bins. (b) The same as in (a) but with the mean wind direction at Das on the x-axis. (c) The same as in (b) but with the mean wind direction at Santa Llocaia on the x-axis. The three graphs have the same y-title and color scale.

Figure 3. For the 163 selected stable days within the study period: (a) Mean daily cycle of temperature at the six AWSs. The x-axis spans from 1200 UTC to 1200 UTC to better interpret the nocturnal dynamics. (b) Temporal evolution of the hourly cooling rate during the nocturnal hours. The nocturnal hours refer to the number of hours from the last registered data before sunset. (c) Probability density estimate for the daily minimum temperature differences between Das and the others AWSs, being ΔT_{min} = T_{min}(DA) - T_{min}(other AWSs). (d) Mean daily cycle of wind direction of the six AWSs. The legend in (b) and (d) is the same as in (a).

Figure 4. Comparison between the evolution of the temperature during the period from 30/09/2011 at 1200 UTC to 02/10/2011 at 1200 UTC, and the results obtained from the MesoNH model. AWS measurements are in solid lines, and MesoNH results are in dashed lines. (a) Comparisons of DA, SL and MR, (b) in ML, LM, CN.

Figure 5. (a) Land surface temperature in a zoom inside domain 2 derived from MODIS satellite at 02/10/2011 0220 UTC. Crosses show the AWSs location. (b) Evolution, from 30/09/2011 at 1200 UTC to 02/10/2011 at 1200 UTC, of the average surface temperature of the entire domain 2, obtained by the MesoNH model every 30 minutes (with the standard deviation), compared with the values obtained from the available nine images of MODIS satellite.

Figure 6. (a) Mean nocturnal surface temperature (01-02/10/2011) between sunset and sunrise, from the mesoscale simulation. (b) Basin-averaged deviation of the surface temperature and the temperature at 1.5 m height from its mean nocturnal temperature between sunset and sunrise, from the mesoscale simulation. (c) Difference between the local spatial deviation of the LST at the end of the night (01-02/10/2011) and at the beginning. The blue polygon notes the area selected as the Cerdanya main valley, also imposing an altitude lower than 1500 m asl. Crosses in (a) and (c) show the AWS locations.

Figure 7. (a) Evolution of the percentage of valley area affected by a cold-air pool, during the night between 1 and 2 October 2011, considering different thresholds $\Delta\tilde{T}(x,y,t) \leq -1.0\ K$, $\Delta\tilde{T}(x,y,t) \leq -2.0\ K$... (b) Evolution of the mean altitude of a threshold of potential temperature of 298 K for the CVL-1 longitudinal axis in blue, and the altitude of the strong stable layers in red. (c) Vertical cross section of the simulated

http://mc.manuscriptcentral.com/joc
Peer Review Only

potential temperature on the longitudinal axis of CVL-1, by the model MesoNH at 01/10/2011 2200 UTC. Black lines show the 298 and 292 K thresholds. (d) The same as (c) at 02/10/2011 0400 UTC.

Figure 8 (a) Horizontal cross section of the simulated wind direction, at 10 m agl, in a zoom inside of domain 2, by the model MesoNH at 02/10/2011 0030 UTC. Crosses show the AWSs location and line shows the longitudinal axis of CVL-1. (b) Vertical cross section of the simulated wind direction on the longitudinal axis of CVL-1, by the same model and at the same time as in (a). Black lines show the potential temperature (lines every 2 K, from 288 K at the bottom up to 302 K at the top).

Figure 9. (a) Temporal evolution of the percentage of grid points below 200 m agl with down-valley flow along the vertical cross-sections of CVL-1, CVL-M and CVL-Q, during the night between 1 and 2 October 2011. Only air columns over a ground surface below 1200 m asl for CVL-1 and between 1200 and 1700 m asl for CVL-M and CVL-Q are considered. Black vertical lines show sunset and sunrise time. (b) Temporal evolution of the mean wind speed for the selected grid points in (a).

Figure 10. (a) Time series of the simulated heat budget at 2.7 m height agl, for a point close to Das, during the night between 1 and 2 October 2011. (b) Average of the vertical profiles of potential temperature budget between 0000 and 0400 UTC on 02/10/2011, for the same point as in (a).

Peer Review Only

Cold-air pool evolution in a wide Pyrenean valley

Laura Conangla[1](*), Joan Cuxart[2], Maria Antonia Jiménez[2], Daniel Martínez-Villagrasa[2], Josep Ramon Miró[3], Davide Tabarelli[4], Dino Zardi[4]

[1] Department of Mining, Industrial and ICT Engineering. Polytechnic University of Catalonia. Manresa, Spain.

[2] Department of Physics. University of the Balearic Islands. Palma de Mallorca, Spain.

[3] Servei Meteorològic de Catalunya. Barcelona, Spain.

[4] Atmospheric Physics Group, Department of Civil, Environmental and Mechanical Engineering, University of Trento, Trento, Italy.

(*) Avinguda de Les Bases de Manresa 61-73, 08242 Manresa, Spain, laura.conangla@upc.edu, +34 93 877 72 76

Peer Review Only

This study on cold-air pool formation in the wide Cerdanya Valley in the Pyrenees mountain range was conducted using available observational information from September 2010 to August 2014. Cold-air pools occur during almost 60% of the nights, mainly during winter. Cold pools develop even under significant synoptic pressure gradients. Additionally, drainage currents transporting air down-valley occur most of the nights. In particular one representative cold-air pool event has been analyzed in detail by a high-resolution mesoscale simulation.

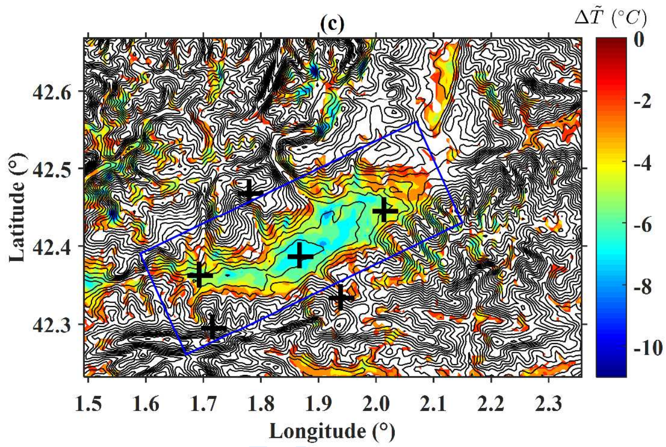

Figure 6. (c) Difference between the local spatial deviation of the LST at the end of the night (01-02/10/2011) and at the beginning. The blue polygon notes the area selected as the Cerdanya main valley, also imposing an altitude lower than 1500 m asl. Crosses show the AWS locations.

Peer Review Only

Table I. Maximum and minimum temperature of the mean daily cycle, thermal amplitude, mean nocturnal cooling rate (during six hours after the sunset) and mean wind direction (from 0000 UTC to 0400 UTC for the night value and from 1000 UTC to 1600 UTC for day value), in the period from 01/09/2010 to 31/08/2014. Standard deviations are in parentheses.

		Tmax (°C)		Tmin (°C)		TA (°C)	NC (°C/h)		WDnight (°)	WDday (°)
	Win.	9.0	(5.4)	-3.2	(4.4)	12.1	0.73	(0.48)	82.2	29.7
DA	Spr.	17.9	(5.9)	4.2	(4.1)	13.7	0.80	(0.42)	103.8	222.7
1097 m	Sum.	24.2	(4.6)	8.4	(3.1)	15.7	0.95	(0.41)	99.7	232.4
	Aut.	11.7	(6.3)	-0.4	(5.7)	12.0	0.75	(0.45)	84.6	330.2
	Win.	8.1	(5.4)	-0.1	(3.7)	8.2	0.28	(0.26)	76.7	2.3
SL	Spr.	16.6	(5.8)	6.8	(4.2)	9.8	0.36	(0.23)	103.1	201.6
1320 m	Sum.	22.9	(4.7)	11.5	(2.9)	11.4	0.35	(0.22)	116.1	204.6
	Aut.	10.9	(6.1)	3.0	(4.7)	7.8	0.32	(0.24)	105.3	234.6
	Win.	12.1	(5.7)	-2.1	(4.1)	14.2	0.81	(0.42)	8.4	189.8
MR	Spr.	20.8	(6.3)	5.8	(4.2)	14.9	0.81	(0.37)	20.3	258.1
1038 m	Sum.	27.6	(5.0)	10.6	(2.9)	17.0	0.94	(0.37)	31.8	256.3
	Aut.	14.8	(6.2)	1.1	(5.4)	13.7	0.78	(0.35)	35.4	224.2
	Win.	0.6	(5.4)	-3.0	(4.7)	3.6	0.09	(0.24)	325.8	250.4
ML	Spr.	8.3	(5.6)	3.5	(5.0)	4.8	0.14	(0.18)	291.1	185.5
2230 m	Sum.	14.4	(4.1)	9.3	(3.5)	5.2	0.14	(0.18)	280.5	185.9
	Aut.	4.3	(5.9)	1.0	(5.2)	3.3	0.08	(0.23)	309.7	210.9
	Win.	4.4	(4.9)	-1.5	(4.0)	5.9	0.21	(0.24)	193.7	294.9
LM	Spr.	12.3	(5.5)	5.0	(4.7)	7.3	0.32	(0.22)	153.6	225.7
1704 m	Sum.	18.9	(4.1)	10.4	(3.4)	8.4	0.37	(0.23)	151.6	221.5
	Aut.	7.7	(6.0)	2.3	(4.8)	5.4	0.19	(0.25)	164.3	263.3
	Win.	0.2	(4.9)	-2.8	(4.7)	3.1	0.10	(0.22)	239.7	263.9
CN	Spr.	8.6	(5.5)	4.1	(5.1)	4.5	0.15	(0.18)	242.1	275.1
2143 m	Sum.	14.5	(3.9)	9.9	(3.5)	4.6	0.17	(0.21)	244.6	282.9
	Aut.	3.4	(5.7)	1.4	(5.2)	2.0	0.08	(0.23)	245.0	258.0

For Peer Review Only

Table II. Percentage of days with cold-air pool, mean strength (S) and mean duration (D) per month, in the period from 01/09/2010 to 31/08/2014, for the temperature difference criteria between Das and Santa Llocaia (T_{DA} - T_{SL}) ≤ - 3.0 °C.
Standard deviation values are in parentheses.

	T_{DA} - T_{SL} ≤ -3.0 °C				
	% days	**S (°C)**		**D (h)**	
Jan.	70.2	-7.4	(2.4)	12.6	(5.1)
Feb.	50.0	-6.7	(2.1)	9.7	(4.3)
Mar.	52.4	-6.1	(1.6)	8.2	(3.1)
Apr.	45.0	-5.8	(1.2)	6.5	(2.7)
May	54.0	-5.4	(1.2)	5.2	(1.9)
Jun.	45.0	-5.5	(1.2)	6.6	(2.1)
Jul.	50.8	-5.3	(1.3)	5.8	(2.3)
Aug.	61.3	-5.7	(1.3)	7.1	(2.8)
Sep	70.8	-6.0	(1.4)	7.8	(2.9)
Oct	65.3	-6.3	(2.0)	9.5	(3.8)
Nov.	55.0	-6.2	(1.9)	10.3	(4.3)
Dec.	80.6	-7.1	(2.1)	13.9	(5.4)

For Peer Review Only

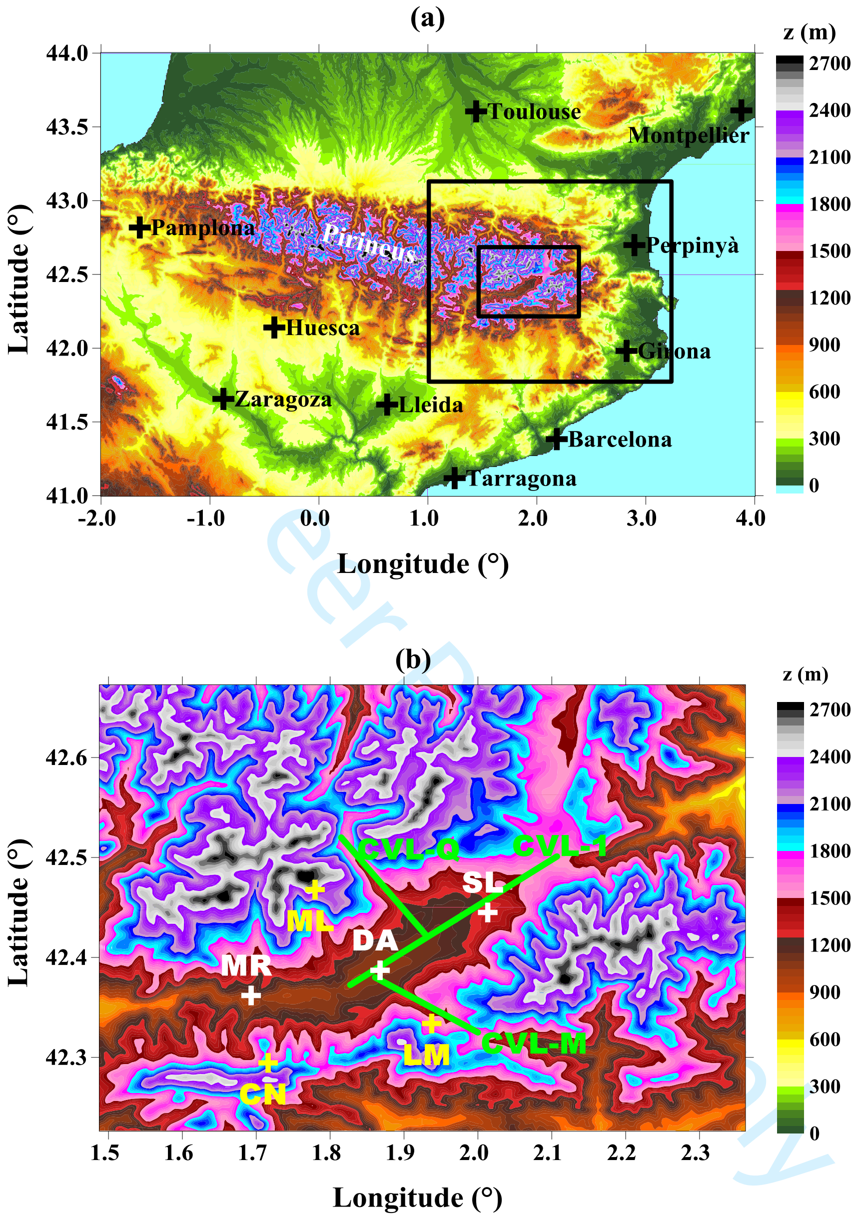

Figure 1. (a) Topographic map of the Pyrenees mountain range of northeastern Spain and the South of France. The two domains for the simulations are shown (domain 2 inside domain 1). (b) Topographic map of domain 2, showing AWS locations (DA, SL, MR, ML, LM, CN) and some longitudinal axes used as vertical cross-sections in the simulation (CVL-1, CVL-M, CVL-Q).

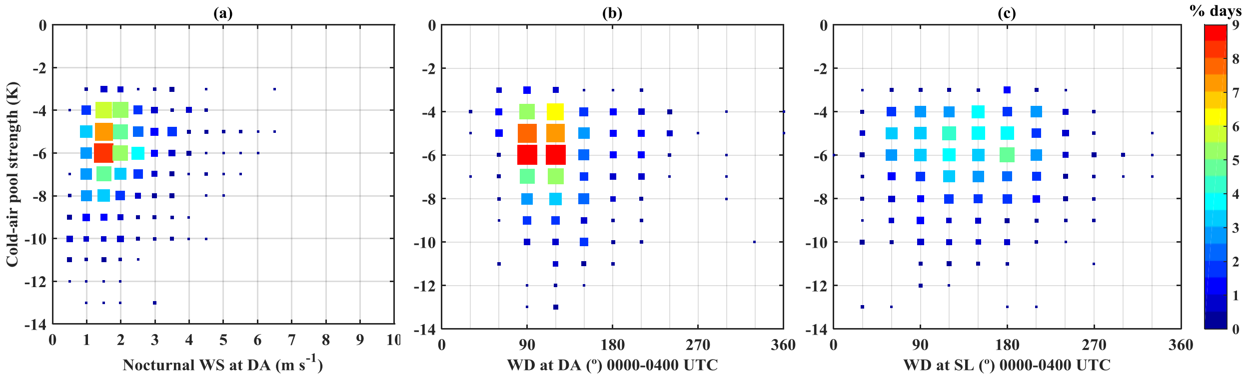

Peer Review Only

Figure 2. (a) Bivariate histogram plot of percentage of cold-air pool days and the mean wind speed from sunset to sunrise at Das versus cold-air pool maximum strength. The temperature difference criterion is T_{DA}-T_{SL} ≤ -3 °C. The size and color of the markers indicate the heights of the bins. (b) The same as in (a) but with the mean wind direction at Das on the x-axis. (c) The same as in (b) but with the mean wind direction at Santa Llocaia on the x-axis. The three graphs have the same y-title and color scale.

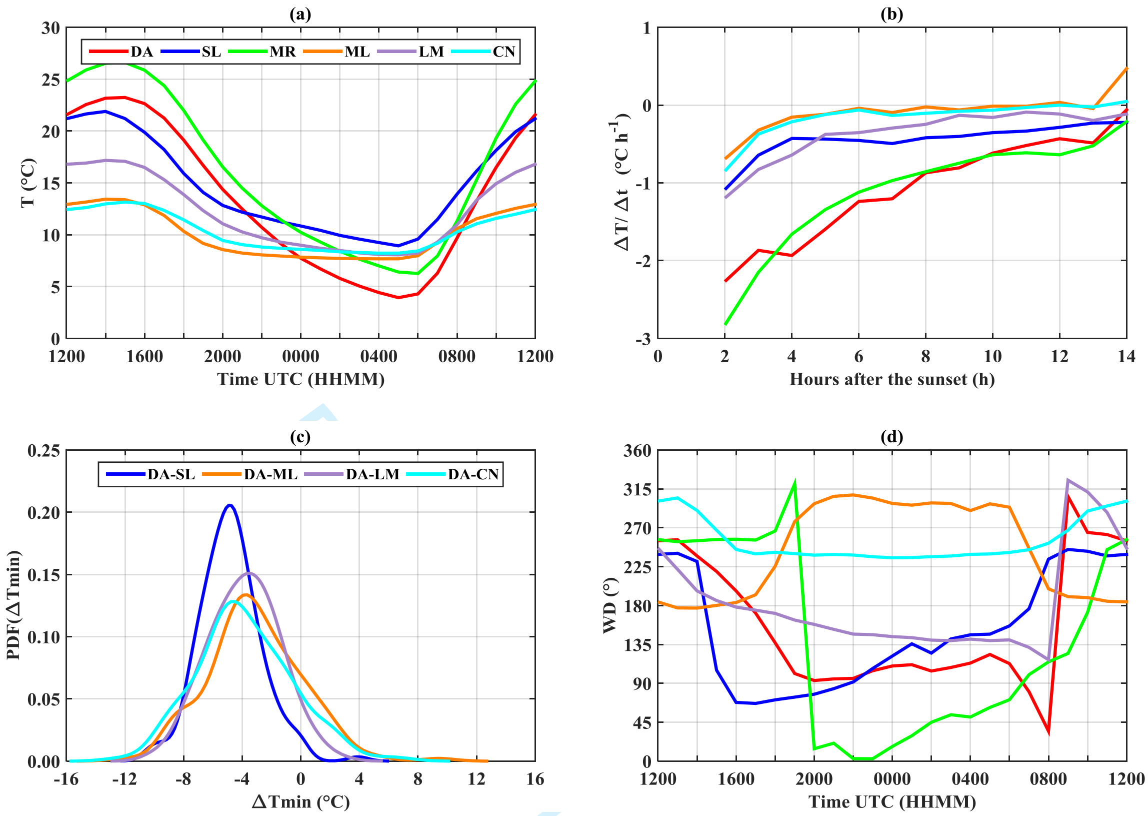

Figure 3. For the 163 selected stable days within the study period: (a) Mean daily cycle of temperature at the six AWSs. The x-axis spans from 1200 UTC to 1200 UTC to better interpret the nocturnal dynamics. (b) Temporal evolution of the hourly cooling rate during the nocturnal hours. The nocturnal hours refer to the number of hours from the last registered data before sunset. (c) Probability density estimate for the daily minimum temperature differences between Das and the others AWSs, being ΔT_{min} = T_{min}(DA) - T_{min}(other AWSs). (d) Mean daily cycle of wind direction of the six AWSs. The legend in (b) and (d) is the same as in (a).

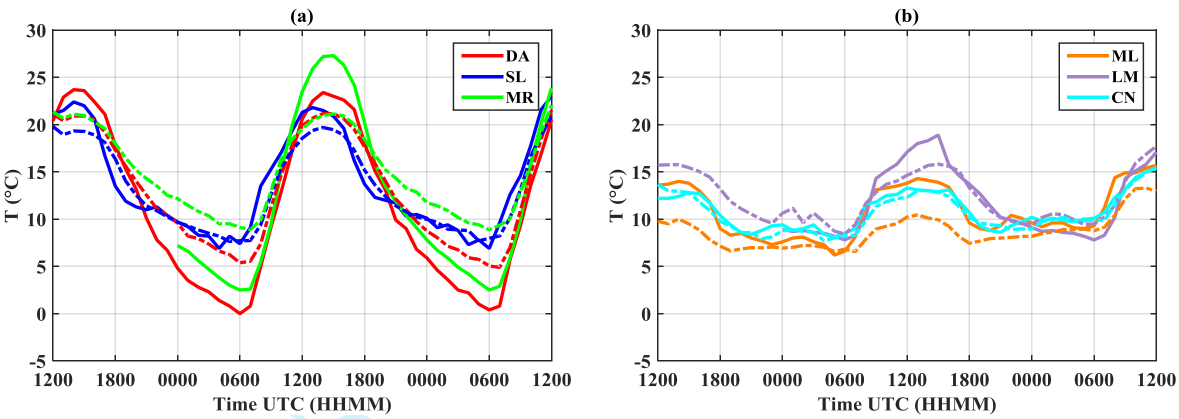

Figure 4. Comparison between the evolution of the temperature during the period from 30/09/2011 at 1200 UTC to 02/10/2011 at 1200 UTC, and the results obtained from the MesoNH model. AWS measurements are in solid lines, and MesoNH results are in dashed lines. (a) Comparisons of DA, SL and MR, (b) in ML, LM, CN.

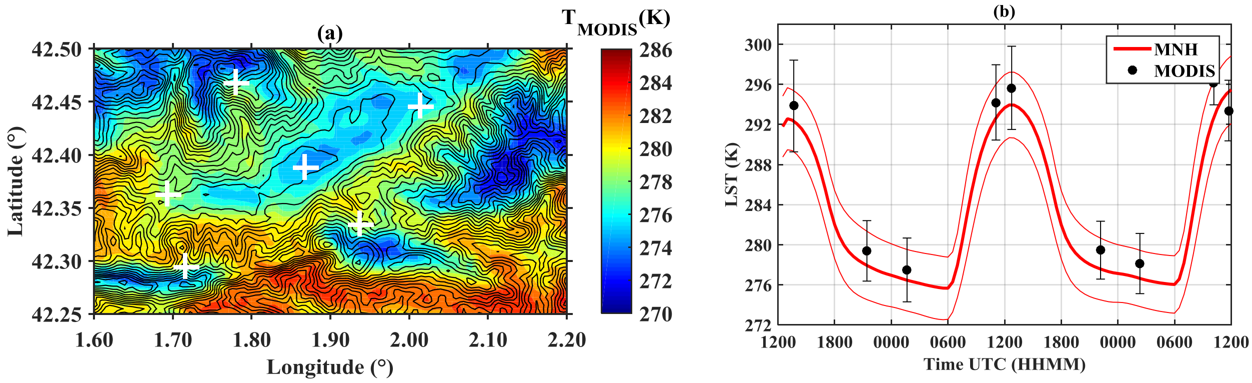

Figure 5. (a) Land surface temperature in a zoom inside domain 2 derived from MODIS satellite at 02/10/2011 0220 UTC. Crosses show the AWSs location. (b) Evolution, from 30/09/2011 at 1200 UTC to 02/10/2011 at 1200 UTC, of the average surface temperature of the entire domain 2, obtained by the MesoNH model every 30 minutes (with the standard deviation), compared with the values obtained from the available nine images of MODIS satellite.

For Review Only

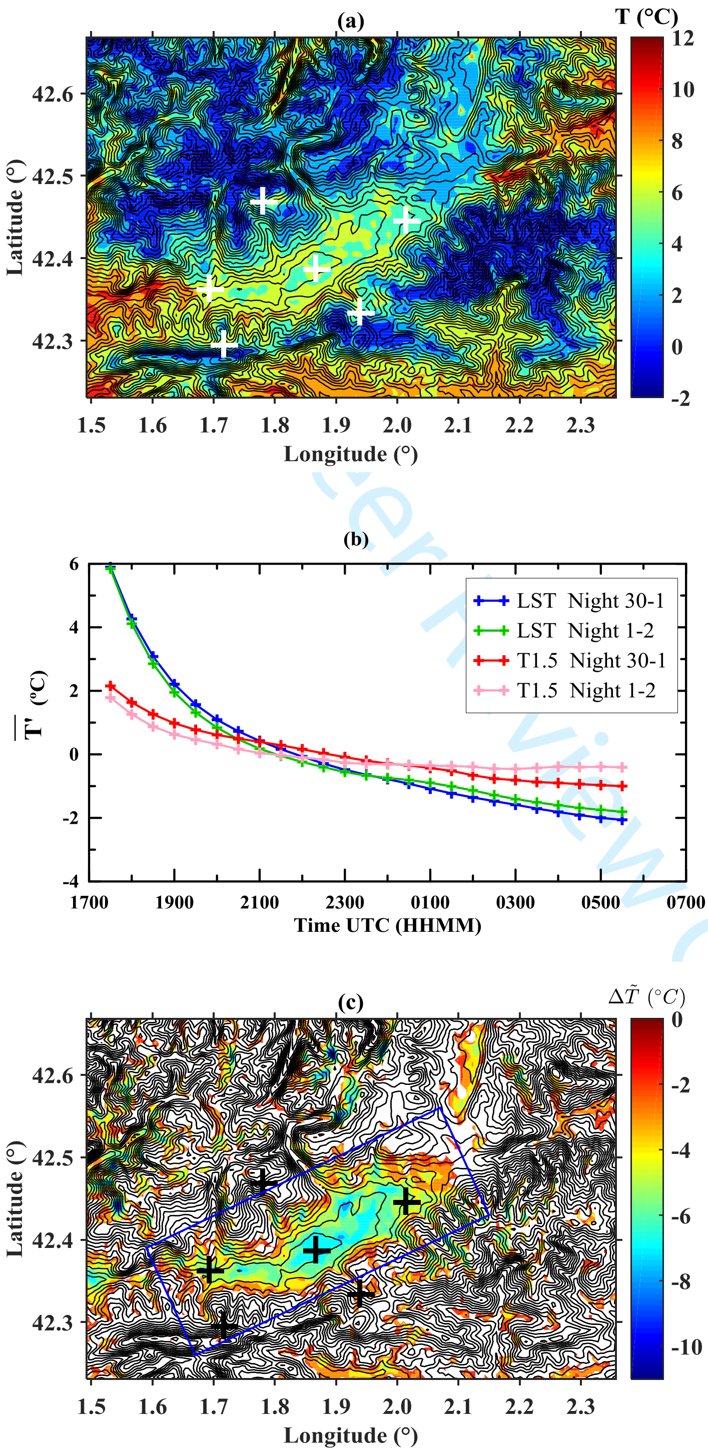
(a)
T (°C)
12
10
8
6
4
2
0
-2
42.6
42.5
42.4
42.3
Latitude (°)
1.5
1.6
1.7
1.8
1.9
2.0
2.1
2.2
2.3
Longitude (°)
(b)
6
4
2
0
-2
-4
$\overline{T'}$ (°C)
LST Night 30-1
LST Night 1-2
T1.5 Night 30-1
T1.5 Night 1-2
1700
1900
2100
2300
0100
0300
0500
0700
Time UTC (HHMM)
(c)
$\Delta\tilde{T}$ (°C)
0
-2
-4
-6
-8
-10
42.6
42.5
42.4
42.3
Latitude (°)
1.5
1.6
1.7
1.8
1.9
2.0
2.1
2.2
2.3
Longitude (°)

Figure 6. (a) Mean nocturnal surface temperature (01-02/10/2011) between sunset and sunrise, from the mesoscale simulation. (b) Basin-averaged deviation of the surface temperature and the temperature at 1.5 m height from its mean nocturnal temperature between sunset and sunrise, from the mesoscale simulation. (c) Difference between the local spatial deviation of the LST at the end of the night (01-02/10/2011) and at the beginning. The blue polygon notes the area selected as the Cerdanya main valley, also imposing an altitude lower than 1500 m asl. Crosses in (a) and (c) show the AWS locations.

Peer Review Only

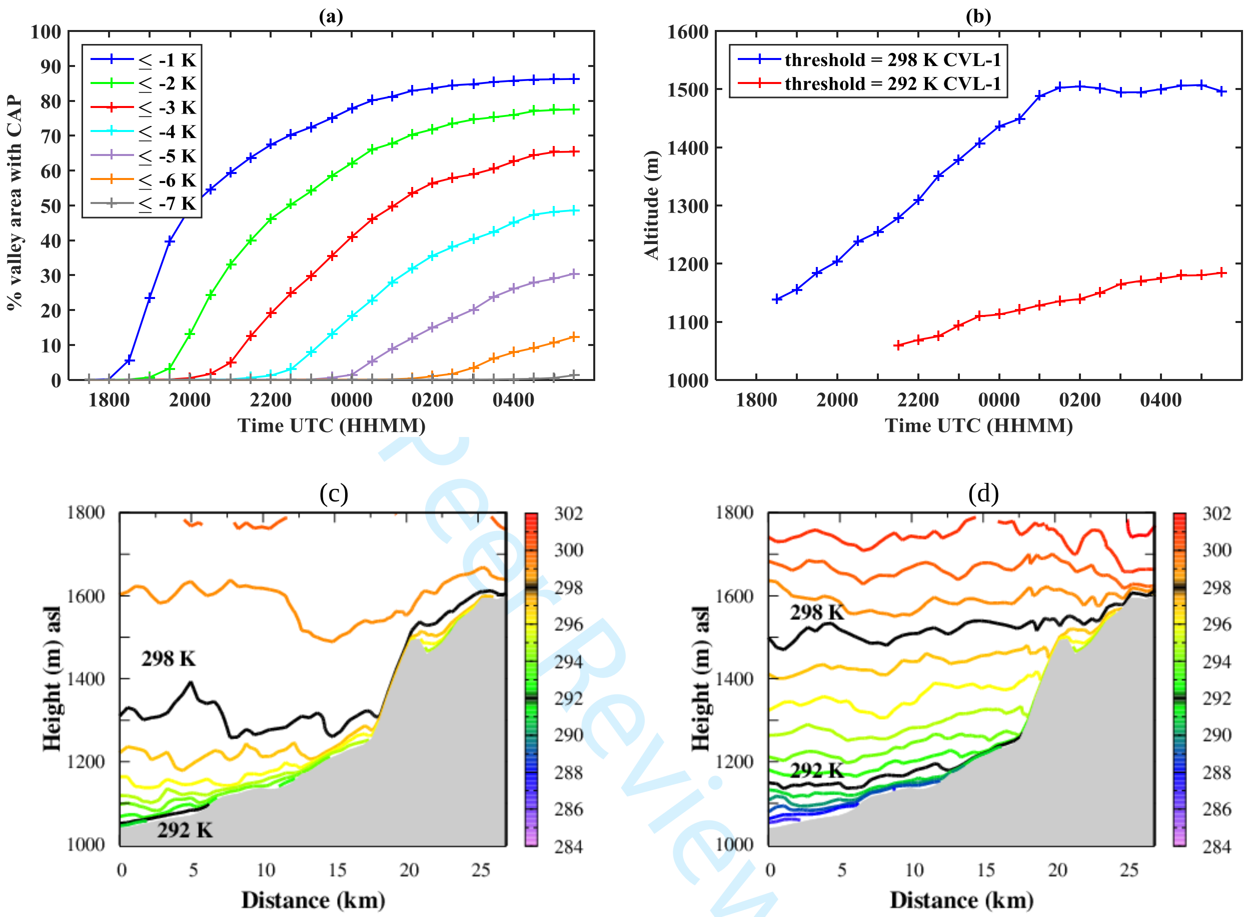

Figure 7. (a) Evolution of the percentage of valley area affected by a cold-air pool, during the night between 1 and 2 October 2011, considering different thresholds $\Delta\tilde{T}(x,y,t) \leq -1.0\ K$, $\Delta\tilde{T}(x,y,t) \leq -2.0\ K$... (b) Evolution of the mean altitude of a threshold of potential temperature of 298 K for the CVL-1 longitudinal axis in blue, and the altitude of the strong stable layers in red. (c) Vertical cross section of the simulated potential temperature on the longitudinal axis of CVL-1, by the model MesoNH at 01/10/2011 2200 UTC. Black lines show the 298 and 292 K thresholds. (d) The same as (c) at 02/10/2011 0400 UTC.

Peer Review Only

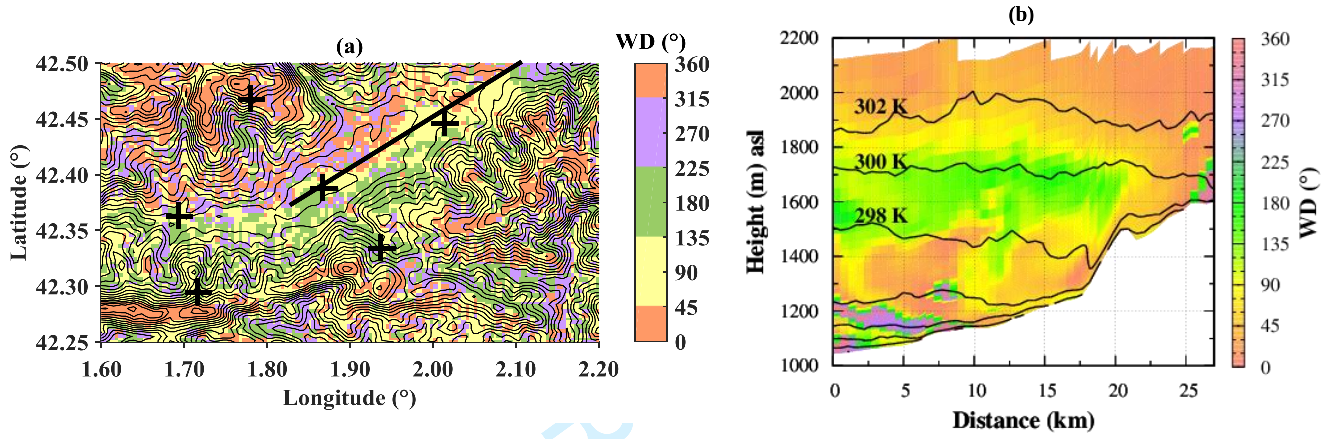

Figure 8 (a) Horizontal cross section of the simulated wind direction, at 10 m agl, in a zoom inside of domain 2, by the model MesoNH at 02/10/2011 0030 UTC. Crosses show the AWSs location and line shows the longitudinal axis of CVL-1. (b) Vertical cross section of the simulated wind direction on the longitudinal axis of CVL-1, by the same model and at the same time as in (a). Black lines show the potential temperature (lines every 2 K, from 288 K at the bottom up to 302 K at the top).

For Peer Review Only

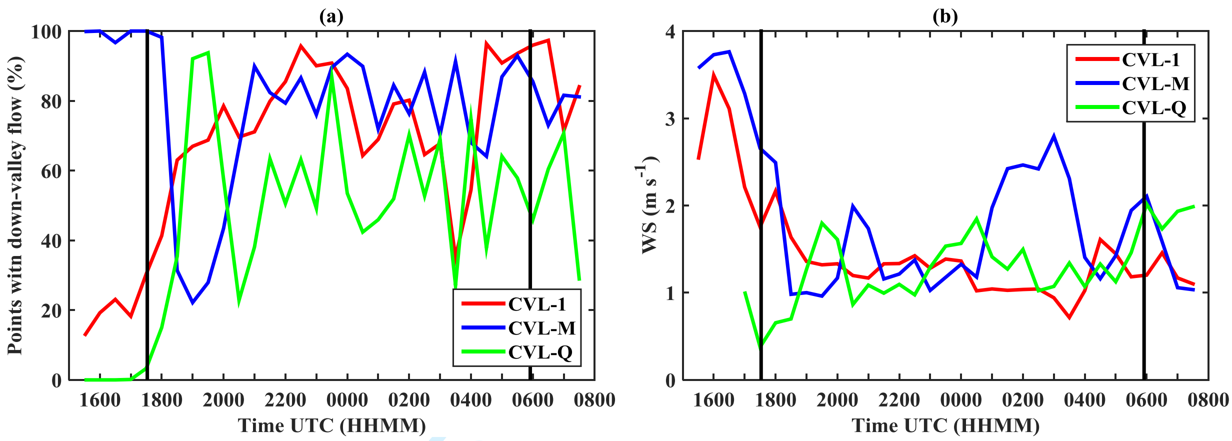

Figure 9. (a) Temporal evolution of the percentage of grid points below 200 m agl with down-valley flow along the vertical cross-sections of CVL-1, CVL-M and CVL-Q, during the night between 1 and 2 October 2011. Only air columns over a ground surface below 1200 m asl for CVL-1 and between 1200 and 1700 m asl for CVL-M and CVL-Q are considered. Black vertical lines show sunset and sunrise time. (b) Temporal evolution of the mean wind speed for the selected grid points in (a).

eview Only

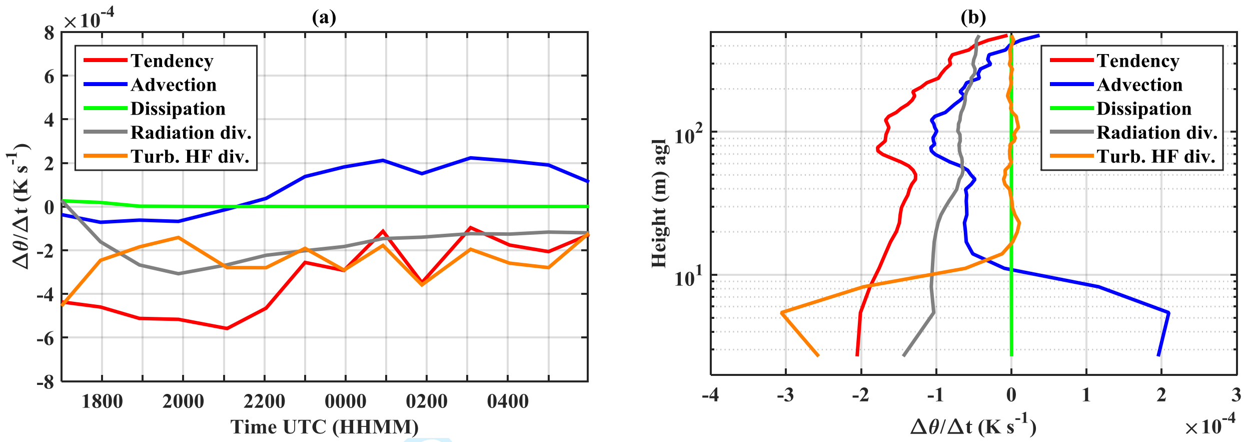

Figure 10. (a) Time series of the simulated heat budget at 2.7 m height agl, for a point close to Das, during the night between 1 and 2 October 2011. (b) Average of the vertical profiles of potential temperature budget between 0000 and 0400 UTC on 02/10/2011, for the same point as in (a).

For Peer Review Only